Nop9 is an RNA binding protein present in pre-40S ribosomes and required for 18S rRNA synthesis in yeast

Nop9 is an RNA binding protein present in pre-40S ribosomes and required for 18S rRNA synthesis in yeast

EMMA THOMSON, JURI RAPPSILBER, and DAVID TOLLERVEY
Wellcome Trust Centre for Cell Biology, University of Edinburgh, Edinburgh EH9 3JR, Scotland

ABSTRACT

Proteomic analyses in yeast have identified a large number of proteins that are associated with preribosomal particles. However, the product of the yeast ORF *YJL010C*, herein designated as Nop9, failed to be identified in any previous physical or genetic analysis of preribosomes. Here we report that Nop9 is a nucleolar protein, which is associated with 90S and 40S preribosomes. In cells depleted of Nop9p, early cleavages of the 35S pre-rRNA are inhibited, resulting in the nucleolar retention of accumulated precursors and a failure to synthesize 18S rRNA. Nop9 contains multiple pumilio-like putative RNA binding repeats and displays robust in vitro RNA binding activity. The identification of Nop9p as a novel, essential factor in the nuclear maturation of 90S and pre-40S ribosomal subunits shows that the complement of ribosome synthesis factors remains incomplete.

Keywords: nucleolus; ribosome synthesis; *Saccharomyces cerevisiae*; RNA binding; pumilio

INTRODUCTION

Ribosomes are large RNP particles containing a single copy of each of four rRNA species and 79 ribosomal proteins. The 80S yeast ribosome is composed of two unequal subunits, a large 60S subunit containing the 25S, 5.8S, and 5S rRNA and a smaller 40S subunit containing only the 18S rRNA species. Three out of the four mature rRNAs, 18S, 5.8S, and 25S, are transcribed as a single 35S pre-rRNA. Synthesis of ribosomes in *Saccharomyces cerevisiae* requires the processing of the 35S pre-rRNA to the mature species (Fig. 1), in addition to the recruitment of the 5S rRNA and ribosomal proteins. Processing of the pre-rRNAs occurs within preribosomal particles that contain, in addition to pre-rRNA and ribosomal proteins, the plethora of processing, modification and assembly factors.

To date, over 180 nonribosomal *trans*-acting factors have been implicated in pre-rRNA processing and ribosome assembly. A disproportionate number of characterized factors are associated with the synthesis of the large subunit, leading to the suggestion that the complement of factors required for small subunit synthesis might be approaching saturation. Factors were characterized as associated with preribosomes through cosedimentation on density gradients or, more recently, by affinity purification of preribosomal particles followed by proteomic analyses (Baßler et al. 2001; Harnpicharnchai et al. 2001; Saveanu et al. 2001, 2003; Dragon et al. 2002; Fatica et al. 2002; Grandi et al. 2002; Schafer et al. 2003). *Trans*-acting factors must associate with preribosomes reasonably stably and/or over long periods of time in order to be so identified. A greater challenge exists in identifying proteins that interact weakly and/or transiently with preribosomes. This is illustrated by the fact that numerous factors implicated in the maturation of preribosomes and processing of pre-rRNA, including most known nucleases, have failed to be identified in association with preribosomal particles.

The previously uncharacterized ORF, *YJL010C*, encodes an essential 77.7-kDa protein, which we have termed Nop9 (nucleolar protein). We identified Nop9 as a potential ribosome synthesis factor from a small number of hits reported from high-throughput affinity purification studies, which identified it in potential association with the ribosome synthesis factors Nsr1 and Nop56 (Hazbun et al. 2003; Krogan et al. 2006). Nop9 has not, however, been identified as a component of any purified preribosomal particle in more than 100 previously published TAP purifications. Nop9 contains multiple pumilio-like putative RNA binding repeats (PUM repeats), which combine to

Reprint requests to: David Tollervey, Wellcome Trust Centre for Cell Biology, University of Edinburgh, Edinburgh EH9 3JR, Scotland; e-mail: d.tollervey@ed.ac.uk; fax: 44-131-650-7040.

Article published online ahead of print. Article and publication date are at http://www.rnajournal.org/cgi/doi/10.1261/rna.747607.

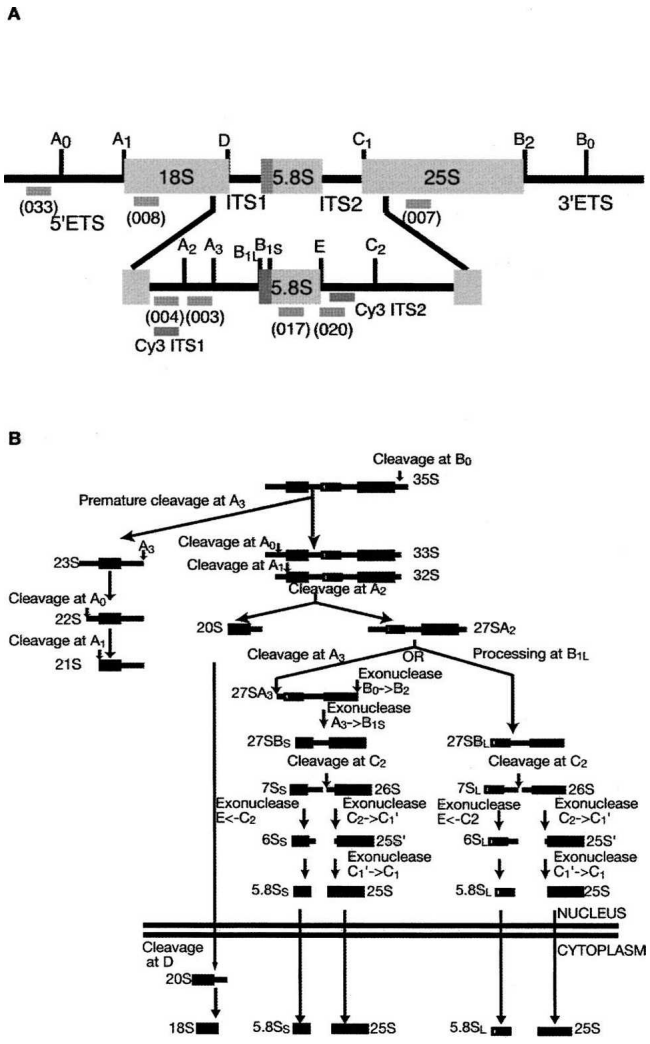

FIGURE 1. Processing pathway in *Saccharomyces cerevisiae*. (*A*) The structure of the 35S rRNA precursor and locations of processing sites. The pre-rRNA encodes the 18S, 5.8S, and 25S rRNAs, which are flanked by the 5′ and 3′ external transcribed spacers (5′ETS and 3′ETS) and separated by internal transcribed sequences 1 and 2 (ITS1 and ITS2). The position of oligonucleotide probes used for Northern hybridization and FISH analysis are shown. (*B*) The pre-rRNA processing pathway. The 35S precursor is generated by cotranscriptional cleavage at site B_0 within the 3′ETS. This is followed by endonucleolytic cleavages at sites A_0 within the 5′ETS, A_1 at the 5′ end of the mature 18S rRNA, and A_2 within ITS1. Premature cleavage at A_3, prior to cleavage of A_0 to A_2, can result in the appearance of the 23S rRNA and subsequent species. Cleavage at A_2 separates the precursors to the 40S and 60S subunits and generates the 20S and $27SA_2$ pre-rRNAs. 20S is subsequently exported from the nucleus to the cytoplasm, where maturation to 18S is completed. The $27SA_2$ pre-rRNA follows one of two alternate pathways: Around 85% is cleaved at the A_3 site within ITS2, followed by 5′-3′ exonucleolytic processing generating the $27SB_s$ pre-rRNA. The remaining 15% is processed at site B_{1L}, which is located 8 nt 5′ to B_{1S}, yielding the $27SB_L$ pre-rRNA. These two alternate forms of 27SB are cleaved within ITS2 at site C_2, yielding 26S pre-rRNA and the long and short forms of 7S. The 7S pre-rRNAs are converted to mature $5.8S_L$ and $5.8S_S$ by a multistep 3′ exonuclease pathway. Maturation of 26S to 25S rRNA similarly proceeds by a two-step 5′ exonuclease pathway.

form an imperfect pumilio-like homology domain. This suggested that Nop9 could display RNA binding activity, increasing the a priori likelihood that it participates in ribosome synthesis.

RESULTS

Nop9 is a component of 90S preribosomes and pre-40S particles

To determine whether Nop9 interacts with preribosomal particles, a Nop9-TAP strain was used (Ghaemmaghami et al. 2003). *NOP9* is essential for viability based on data from the systematic deletion project in *S. cerevisiae* (Winzeler et al. 1999). The growth of the strain expressing only tagged Nop9 was indistinguishable from an otherwise isogenic wild type (data not shown), showing the Nop9-TAP fusion to be functional. Total cell extract from the Nop9-TAP strain was used for sucrose density gradient analysis and affinity purification (Fig. 2). The sedimentation pattern of Nop9-TAP was compared with the pre-rRNA components of preribosomes on a 10%–50% sucrose gradient. Western blot analysis showed that Nop9-TAP sedimented in the 40S to 90S region, with two peaks (Fig. 2A, c). The upper Nop9-TAP peak (fractions 8–10) may reflect an association with pre-40S particles, as judged by cosedimentation with 20S pre-rRNA (Fig. 2A, b,c). The lower Nop9-TAP peak (fractions 13–15) cosedimented with the 23S, $27SA_2$, 35S, and 33/32S pre-rRNA species (Fig. 2A, a,c). This could correspond to the association of Nop9-TAP with 90S, pre-60S, and/or pre-40S particles containing 23S RNA.

To clarify the nature of the association of Nop9 with preribosomes, immunoprecipitation was performed utilizing the Nop9-TAP strain, and the associated RNA and proteins were identified. Nop9-TAP coprecipitated the 20S pre-rRNA and, less efficiently, 35S pre-rRNA (Fig. 2B, a,c). Consistent with its incorporation into pre-40S particles, Nop9-TAP coprecipitated the 22S and 23S RNAs (Fig. 2B, a). These species are classed as aberrant intermediates in 18S rRNA maturation but are enriched in association with other ribosome synthesis factors, conceivably as part of the mechanism targeting them for degradation (Allmang et al. 2000). In contrast, pre-rRNAs on the pathway of 60S ribosome synthesis ($27SA_2$, 7S, and 6S) were not detectably enriched in Nop9-TAP precipitation compared with the untagged control (Fig. 2C, a–c), and neither were mature rRNAs or the snoRNAs that were tested (Fig. 2B,C). Together these data show that Nop9 is associated with both 90S preribosomes and pre-40S particles. A number of early-acting 90S synthesis factors, which fail to be incorporated into pre-40S particles, efficiently precipitate the 5′ETS-A_0 fragment (Schafer et al. 2003). This indicates that these factors associate with the 5′ETS and are released from the preribosomes by the first cleavage reaction. Nop9-TAP does not efficiently precipitate the 5′ETS-A_0 (Fig. 2C, a)

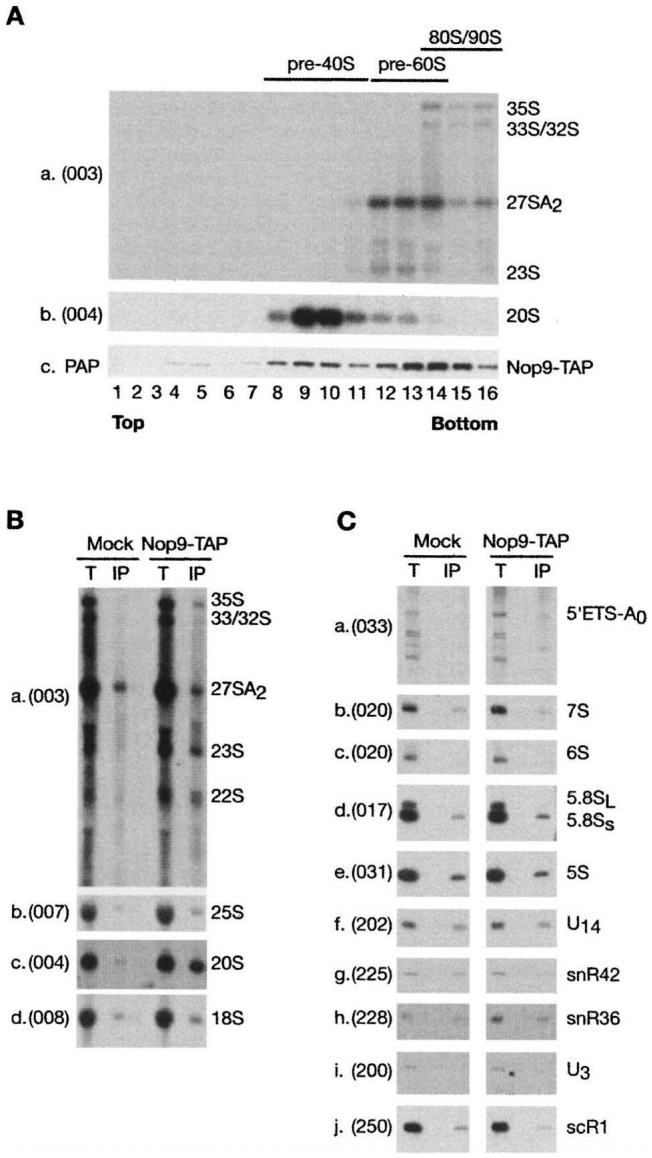

FIGURE 2. Nop9 associates with preribosomal particles. (*A*) Cell lysate from a strain expressing Nop9-TAP was loaded on a 10%–50% sucrose gradient. (*a*) Northern hybridization with a probe (003) that hybridizes to the 35S, 33/32S components of 90S preribosomes, the $27SA_2$ component of pre-60S particles, and 23S rRNA. (*b*) Northern hybridization with probe 004 against the 20S pre-rRNA component of pre-40S particles. (*c*) Western blotting using peroxidase–anti-peroxidase (PAP) that recognizes the prot A region of the TAP tag from Nop9-TAP. Fraction numbers are indicated, where 1 is the top gradient fraction. (*B*, *C*) Northern analysis of RNAs coprecipitated with Nop9-TAP or from mock precipitated, untagged control strains. Cell lysates from a strain expressing Nop9-TAP were incubated with IgG sepharose and Nop9-containing particles were obtained by release from the prot A tag with TEV protease. RNA was prepared from total cell extracts (total) and immunoprecipitated samples (IP). (*B*) RNA was glyoxyl denatured, and separated on a 1.2% agarose gel to resolve high-molecular-weight species. (*C*) To analyze low-molecular-weight species, RNA was separated on a denaturing 6% polyacrylamide/8.3 M urea gel. In *B* and *C*, total RNA loaded corresponds to 2% of the amount used as input for immunoprecipitations. Following migration RNAs were transferred to a nylon membrane and hybridized with the 5′-labeled oligonucleotide probes shown in parenthesis on the *left* of gel panels.

but efficiently coprecipitates 20S pre-rRNA, showing that it binds, directly or indirectly, to the region of the pre-rRNA that is retained in the 20S pre-rRNA.

A two-step TAP-purification was performed to determine the protein composition of Nop9-TAP–associated particles. Coprecipitated proteins were separated by one-dimensional SDS-PAGE. The entire lane was sliced into five fractions, each containing many proteins, and analyzed by mass spectrometry. Known ribosome synthesis factors identified in the Nop9-TAP precipitate are listed in Table 1 (for a complete list of peptides identified and the corresponding proteins, see Supplemental Table 1; http://www.wcb.ed.ac.uk/tollervey). Thirty-one proteins identified as coprecipitating with Nop9-TAP are characterized 90S preribosomal components, including components of the UTP-A, UTP-B, and UTP-C subcomplexes (Krogan et al. 2006; Perez-Fernandez et al. 2007). Additionally, seven of the core snoRNP protein components, which mediate covalent modification on the 35S pre-rRNA, coprecipitated with Nop9-TAP. Three proteins associated with pre-40S particles, Enp1p, Dim1p, and Tsr1p, were also identified in the Nop9-TAP purification. In addition, we identified a number of characterized 60S subunit synthesis factors that we speculate associated with the pre-rRNA prior to cleavage at site A_2. Together, the sedimentation and affinity purification data demonstrate that Nop9-TAP is associated with 90S and pre-40S particles.

Generation and characterization of a conditionally expressed allele of *NOP9*

As *NOP9* is essential, a conditional allele was constructed at the chromosomal *NOP9* locus by placing the expression of a triple HA-fusion under control of the glucose-repressed *GAL1* promoter. On complete, galactose containing media, the growth of the wild-type strain was indistinguishable from the *GAL::3HA-nop9* allele (data not shown). Eight hours after transfer from galactose- to glucose-containing media, growth of the *GAL::3HA-nop9* strain began to slow relative to the wild type (Fig. 3A). Levels of 3HA-Nop9 were followed by Western analysis during the depletion time-course (Fig. 3B). 3HA-Nop9 levels detectably decreased 4 h after transfer to glucose medium, with a more substantial decrease after 8 h, coincident with the appearance of the growth defect.

Nop9 is required for pre-rRNA processing

To determine whether Nop9 is required for ribosome biogenesis, in vivo labeling of cells with [8-^{3}H] adenine was performed. The *GAL::3HA-nop9* strain and isogenic wild type, which are prototrophic for adenine, were pregrown in glucose containing minimal medium lacking adenine for 8 h, to deplete Nop9. Cells were then labeled with [8-^{3}H] adenine for 2 min and chased with a large excess of cold adenine.

Adenine incorporation into pre-rRNA in the Nop9-depleted strain was reduced approximately twofold relative to the wild type, as estimated from the relative exposures required to give equal signals (Fig. 4), probably as a consequence of the reduced growth rate. In addition, synthesis of the 18S rRNA was inhibited relative to synthesis of the 25S, 5.8S, and 5S rRNAs (Fig. 4A, b, B, b). 18S rRNA continues to be synthesized at low levels in the Nop9-depleted strain, most likely due to leakiness of the *GAL1* promoter. The 35S primary transcript normally undergoes rapid endonuclease cleavage at sites A_0 to A_2 to generate the 20S and $27SA_2$ pre-rRNAs (see Fig. 1). In Nop9-depleted cells, 35S persisted at later chase time points (Fig. 4A, a,b), while accumulation of the 20S and 27SA pre-rRNAs was reduced. In many strains blocked for cleavage at sites A_0 to A_2, processing within ITS1 continues through direct cleavage of the 35S pre-rRNA at A_3. This generates the 23S RNA and the $27SA_3$ pre-RNA, which is rapidly processed to 27SB. The 27SB pre-rRNA continued to be synthesized in Nop9-depleted cells, and a low level of the 23S RNA was detected.

Steady-state levels of precursor and mature rRNAs were analyzed by Northern hybridization of total RNA extracted during the time-course of 3HA-Nop9 depletion (Fig. 5). Following 4 h of growth on glucose-containing YPD media, the 35S pre-rRNA showed modest accumulation, but this may be due in part to the effects of nutritional upshift that normally follows a shift from galactose to glucose medium. After transfer for 8 h, 35S pre-rRNA was further elevated accompanied by reduced levels of 33S, 32S, $27SA_2$, and 20S pre-rRNAs (Fig. 5A, a,c). The fragment of the 5′-ETS released by endonucleolytic cleavage at A_0 (5′ETS-A_0) also disappears concomitant with the loss of 33S pre-rRNA

TABLE 1. Ribosome synthesis factors associated with Nop9-TAP

Protein	Preribosome subcomplex	Number of unique peptides	Sequence coverage (%)
Nan1	UTP-A	10	14
Utp4	UTP-A	9	14
Utp5	UTP-A	1	1
Utp8	UTP-A	5	8
Utp9	UTP-A	1	2
Utp10	UTP-A	18	10
Utp15	UTP-A	5	14
Pwp2	UTP-B	9	12
Utp6	UTP-B	3	6
Utp13	UTP-B	6	10
Utp21	UTP-B	4	4
Utp18	UTP-B	1	3
Utp22	UTP-C	19	20
Rrp7	UTP-C	1	2
Sof1	U3 snoRNP, 90S	1	3
Nop1	C/D snoRNP, 90S	12	52
Nop58	C/D snoRNP, 90S	13	33
Sik1	C/D snoRNP, 90S	9	21
Cbf5	H/ACA snoRNP, 90S	4	9
Gar1	H/ACA snoRNP, 90S	2	19
Nhp2	H/ACA snoRNP, 90S	2	18
Nsr1	90S	10	24
Mrd1	90S	14	18
Esf1	90S	3	6
Utp7	90S	1	3
Bfr2	90S	3	5
Bms1	90S	6	6
Fcf2	90S	1	9
Rok1	90S	1	2
Mpp10	90S	2	3
Dhr2	90S	1	1
Prp43	90S + pre-60S + pre-40S	3	4
Rrp12	90S + pre-60S +pre-40S	4	4
Rrp5	90S + pre-60S	42	30
Rrp9	90S + pre-60S	2	4
Has1	90S + pre-60S	3	8
Enp2	90S + pre-60S	5	8
Enp1	90S + pre-40S	3	6
Tsr1	pre-40S	2	2
Dim1	Pre-40S	1	3
Dbp2	Pre-60S	3	6
Erb1	Pre-60S	4	5
Nsa2	Pre-60S	1	3
Nog1	Pre-60S	1	2
Nop4	Pre-60S	1	1
Mak21	Pre-60S	6	6
Nug1	Pre-60S	1	1
Arx1	Pre-60S	1	3

Ribosome synthesis factors purified with Nop9-TAP and subsequently identified by tandem MS/MS mass spectrometry. Peptides reported had statistically highly significant identification scores (see Materials and Methods), so single peptides are sufficient to unambiguously identify the source protein independent of the percentage coverage.

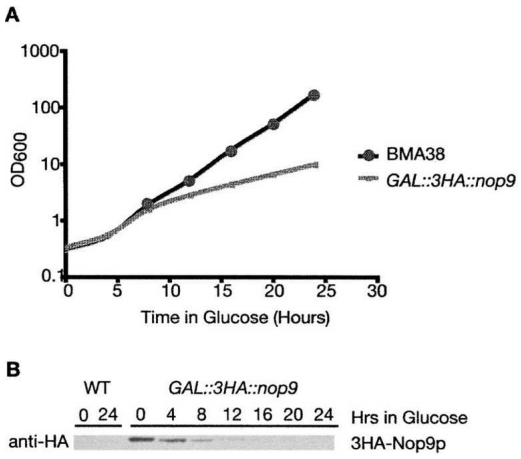

FIGURE 3. Depletion of 3HA-Nop9 inhibits cell growth. (*A*) Growth rate of wild-type and *GAL::3HA-nop9* strains following transfer from permissive galactose containing medium to nonpermissive glucose containing medium for the times indicated. Cells were maintained in exponential growth throughout the time course by addition of prewarmed medium. The value of the OD takes into consideration any dilution factor. (*B*) Western analysis of 3HA-Nop9 depletion. 3HA-Nop9 was decorated with a rabbit anti-HA primary antibody, which was subsequently detected using an anti-rabbit igG coupled to horseradish peroxidase.

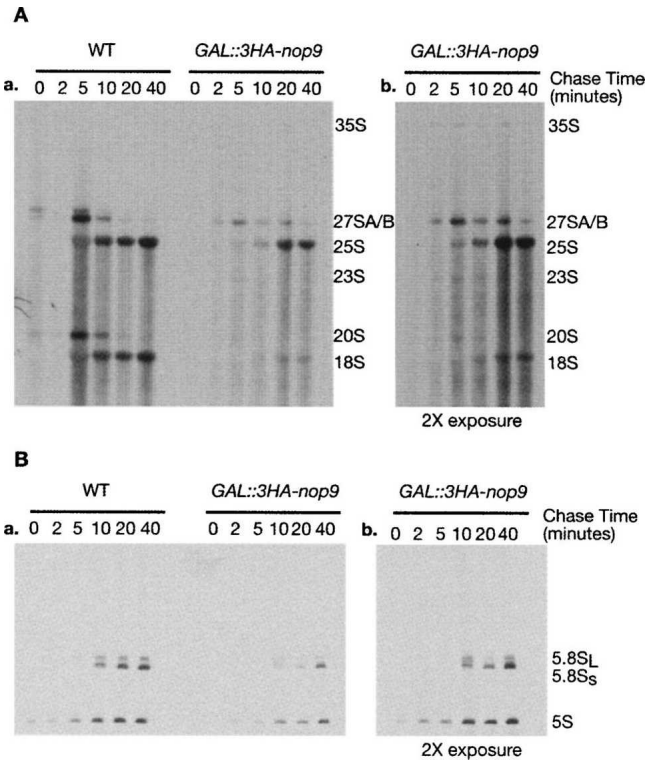

FIGURE 4. Depletion of Nop9 inhibits synthesis of 18S rRNA. Wild-type and *GAL::3HA-nop9* strains were transferred to glucose containing minimum medium (lacking adenine) for 8 h, following growth on galactose containing minimum medium (lacking adenine). Cells were pulse labeled with [8-^{3}H] adenine for 2 min followed by a chase with a large excess of cold adenine for the times indicated. (*A*) High-molecular-weight RNA was glyoxyl denatured and resolved on a 1.2% agarose gel. (B) Low-molecular-weight RNA was separated on a 6% polyacrylamide/8.3 M urea gel. In *A* and *B*, *a* shows the same exposure for the wild-type and *GAL::3HA-nop9* samples, while *b* shows a twofold longer exposure of the *GAL::3HA-nop9* samples.

(Fig. 5B, a). The level of the 23S RNA was elevated, following 4 h of growth on glucose containing medium, and continues to show moderate accumulation until 20 h, where levels begin to decrease (Fig. 5A, a), presumably reflecting reduced pre-rRNA transcription due to the falling growth rate. Levels of the precursors on the pathway of 60S synthesis (27SB, 7S, and 6S) were little affected by depletion of Nop9 (Fig. 5A, b, B, b,c). In agreement with the loss of 18S synthesis seen in pulse chase analysis, steady-state levels of 18S rRNA decreased (Fig. 5A, e), while the 5.8S and 25S rRNAs remained unaffected (Fig. 5A, d, B, d). The snoRNAs U3, U14, and snR30 are required for the early pre-rRNA cleavage steps that are inhibited by loss of Nop9. The levels of snoRNAs were therefore assessed throughout the depletion of Nop9 (Fig. 5C). No alterations were observed in the accumulation of any snoRNA tested, including representatives of both major classes, the H/ACA and C/D box containing snoRNAs. Together the data show that depletion of Nop9 specifically blocks pre-rRNA cleavage at sites A_0, A_1, and A_2, resulting in the loss of 18S rRNA synthesis.

Nop9 is a nucleolar protein

Pre-40S particles are generated in the nucleolus and rapidly exported to the cytoplasm, where maturation of 18S rRNA from 20S pre-rRNA is completed (Udem and Warner 1973). Since Nop9-TAP associates with 20S pre-rRNA, we determined its localization to assess whether it is exported to the cytoplasm with the pre-40S particle. For this, a C-terminal Nop9-GFP fusion was created by integration at the endogenous *NOP9* locus. The growth of the tagged strain was indistinguishable from otherwise isogenic wild type, indicating the fusion protein was functional (data not shown). The nucleolus was identified in fixed cells by indirect immunofluorescence using a mouse anti-Nop1p antibody (Wu et al. 1998) and a goat anti-mouse alexa-fluor-555 conjugated secondary antibody. The nucleoplasm was visualized with DAPI, present in the mounting agent. Nop9-GFP colocalized with Nop1p but was largely excluded from the DAPI-stained nucleoplasm and displayed no detectable cytoplasmic signal (Fig. 6A). This pattern of localization is consistent with the association of Nop9 with 90S preribosomes and early, nucleolar pre-40S particles prior to their export to the cytoplasm.

Nop9 is required for release of pre-40S particles from the nucleolus

The localization of pre-rRNA species was assessed during Nop9 depletion to determine whether the transit of preribosomal particles from the nucleolus to the nucleoplasm

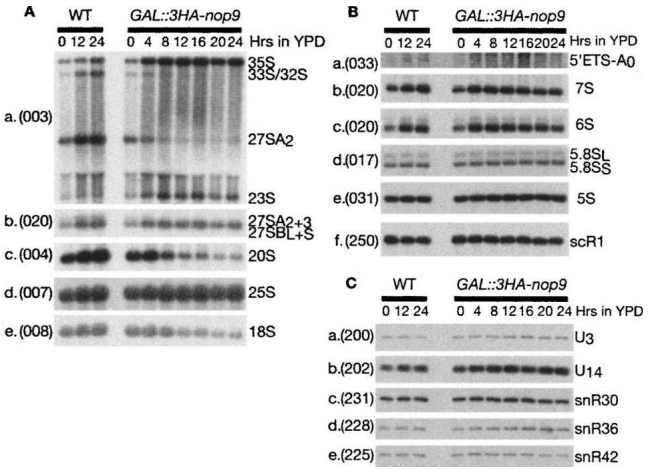

FIGURE 5. Nop9 is required for the processing of early precursors and the synthesis of 18S rRNA. Total RNA was extracted during growth on galactose medium (0 h time point) and at the intervals indicated, following transfer to glucose medium. (*A*) Northern analyses of high-molecular-weight RNA species resolved on a 1.2% agarose gel following glyoxyl denaturation. (*B*, *C*) Northern analyses of low-molecular-weight RNA species resolved on a 6% polyacrylamide/8.3 M urea gel. The same RNA preparations are used for each analysis; 4 μg of total RNA was used for each gel. Oligonucleotide probes used for hybridization are indicated in parenthesis on the *left* of each panel.

and/or cytoplasm was affected. The localization of pre-40S particles was determined by fluorescence in situ hybridization (FISH), using a Cy-3–labeled oligonucleotide probe complementary to a 50-nucleotide (nt) sequence present at the 5′ end of ITS1, which is retained in the 20S pre-rRNA (for position of probes, see Fig. 1A). Localization was analyzed in wild-type and *GAL::3HA-nop9* strains under permissive (Fig. 6B, a,b) and nonpermissive (Fig. 6B, c,d) conditions. Under permissive conditions, the Cy3 signal of ITS1 was found in the nucleolus, nucleoplasm, and cytoplasm, with nucleolar enrichment, in both wild-type and mutant strains (Fig. 6B, a,b). This is consistent with previous reports that the 20S pre-rRNA is exported through the nucleoplasm and nuclear pore complex (NPC) to the cytoplasm, prior to final maturation to 18S rRNA (Udem and Warner 1973). Following a shift to nonpermissive, glucose medium for 8 h, Nop9-depleted cells showed an increase in nucleolar Cy3 signal with a concomitant decrease in nucleoplasmic and cytoplasmic signals (Fig. 6B, d). We conclude that following depletion of Nop9, preribosomal particles in which the pre-rRNA components retain the D-A_2 region accumulate in the nucleolus. The images presented in Figure 6 have been computationally deconvolved from multiple optical sections, allowing a degree of subnucleolar structure to be resolved. However, the subnucleolar distribution of the ITS1 probe was not clearly different between wild-type and Nop9-depleted cells, and no clear focus of staining was observed.

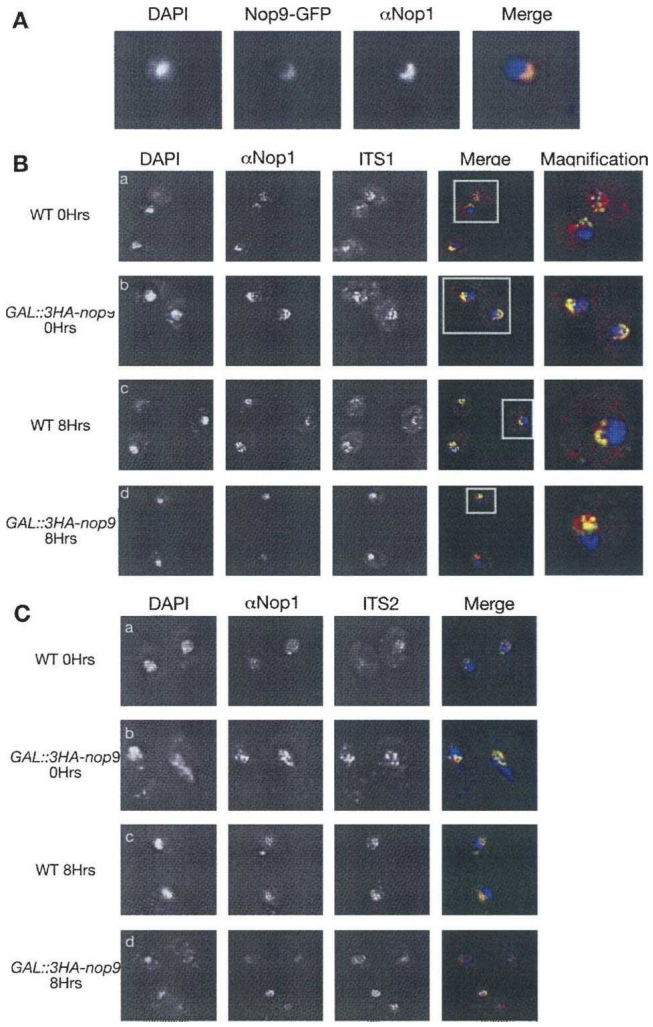

FIGURE 6. Nop9 is a nucleolar protein required for the nucleocytoplasmic export of the pre-40S subunit. (*A*) A strain expressing an endogenously tagged Nop9-GFP fusion protein (green in merge), expressed under its own promoter was fixed in paraformaldehyde and spheroplasted with zymolase. The nucleolus was visualized using an anti-Nop1 antibody that was subsequently recognized by an alexafluor (555) conjugated secondary antibody (red in merge). The nucleoplasm was visualized by DAPI (blue in merge). The green signal was entirely contained within the region decorated by anti-Nop1. (*B*, *C*) Wild-type and *GAL::3HA-nop9* strains were pregrown in galactose and shifted for 8 h to glucose containing media. Cells were fixed in paraformaldehyde and spheroplasted. Fluorescent in situ hybridization (FISH) was performed using Cy-3–labeled probes (red in merge), complementary to the 5′ end of ITS1 (*B*) or the 5′end of ITS2 (*C*). In addition, the nucleolar marker Nop1p was visualized by indirect immunofluorescence using an anti-Nop1 antibody followed by fluorescently conjugated (Alexafluor 488) secondary antibody (green in merge). The nucleoplasm was stained with DAPI, present in the mounting media. This figure shows a single optical section from a deconvolved stack. In *B*, the region outlined by the white square is magnified in the final column.

To assess the effects of depletion of Nop9 on the intracellular transport of pre-60S particles, we used a probe directed against the 5′ end of ITS2, which is retained in the 27SB and 7S pre-rRNAs (Fig. 6C). No difference in the ITS2 signal was seen in Nop9-depleted cells compared with the wild type (Fig. 6C, c,d).

Nop9-depleted cells are defective in the maturation pre-40S particles, and these results indicate that this is associated with a failure in their release from the nucleolus to the nucleoplasm. In contrast, pre-60S particles continue to be efficiently matured and exported to the cytoplasm.

Nop9 displays in vitro RNA binding activity

Nop9 contains a pumilio-like domain, which contains multiple, potential RNA binding sites (Fig. 7A). In vitro RNA binding assays were therefore performed using ^{35}S-labeled, in vitro transcribed, and translated Nop9. Substantial binding of ^{35}S-labeled Nop9 was seen with either poly(A)-sepharose or poly(U)-sepharose, with an apparent preference for polyU. The protein A–sepharose control showed no binding of [^{35}S] Nop9 (Fig. 7B). To assess the specificity of Nop9 RNA binding, the D-A_2 region, present at the 5′ end of ITS1, was in vitro transcribed in the presence of biotinylated UTP, as was a highly structured $tRNA^{Met}$. Transcripts were purified and bound to streptavidin agarose, followed by incubation with [^{35}S] Nop9. The bound and unbound fractions of Nop9 are shown, where equivalent amounts of each fraction of the preparation were loaded. Nop9 convincingly bound both the D-A_2 fragment and $tRNA^{Met}$ (Fig. 7C). We conclude that Nop9

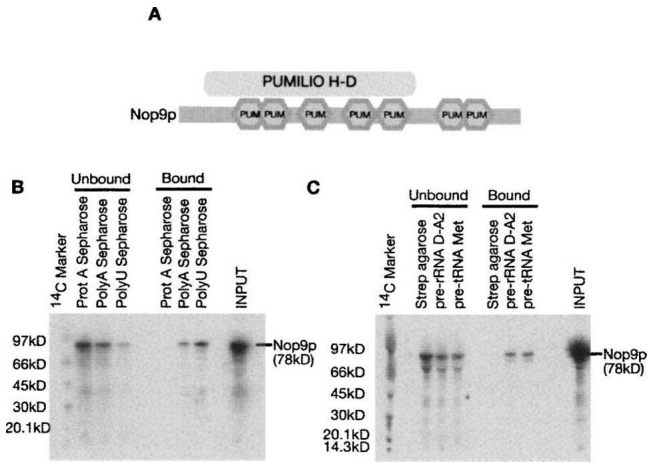

FIGURE 7. Nop9 displays in vitro RNA binding activity. (*A*) Sequence analysis, using PROSITE, suggested that Nop9 contains a Pumilio homology domain (HD) stretching from amino acid residues 23–435, and seven pumilio RNA binding repeat profiles (PUM) located at residues 92–127, 128–163, 188–223, 286–326, 369–407, 511–548, and 549–587. (*B*) [^{35}S]-labeled Nop9, generated from a TnT reaction, was incubated with protein A–sepharose, poly(*A*)-sepharose, and poly(*U*)-sepharose. Equivalent amounts of the proteins recovered from bound and unbound fractions along with total input were separated on a 4%–12% Bis-tris gradient acrylamide gel and visualized by autoradiography. (*C*) [^{35}S]-labeled Nop9 was incubated with streptavidin agarose alone or with streptavidin agarose loaded with biotinylated tRNA^{met} or biotinylated pre-rRNA (D-A_2) fragments. Following incubation, proteins were recovered from bound and unbound fractions and equivalent amounts were run along with the input. Proteins were visualized by autoradiography.

shows robust RNA binding activity, but clear sequence-specificity was not exhibited in vitro.

DISCUSSION

The development of rapid and efficient affinity purification techniques has allowed the identification of numerous, novel, *trans*-acting factors required for ribosome biogenesis (Rigaut et al. 1999). However, many factors required for the maturation of ribosomal subunits, including most of the nucleases, have failed to be recovered in stable association with preribosomal particles. This suggested that factors transiently or weakly associate with preribosomes might have failed to be identified by most current affinity-purification methods.

In excess of 100 affinity purifications have been reported using characterized ribosome synthesis factors as bait proteins, but Yjl010c/Nop9 was not identified in any of these analyses. Despite this, the data presented here establish that Nop9 is indeed a component of late 90S and early pre-40S ribosomal particles and plays an essential role in their maturation. Sucrose density gradients and analyses of protein and RNA coprecipitation support the association of Nop9-TAP with 35S and 20S pre-rRNAs and with numerous previously characterized 90S and pre-40S associated ribosome synthesis factors. It is unclear exactly why Nop9 itself failed to be identified in any previous purifications of preribosomal particles, but it is notable that the identification of coprecipitating proteins reported here required the use of over 20 L of culture of exponentially growing yeast cells. The very low yield of preribosomes associated with Nop9 (and vice versa) may reflect its transient and/or weak association with the preribosomes. We succeeded in purifying Nop9-associated preribosomes at a physiological salt concentration (100 mM KCl) but failed to detect this association under more stringent conditions (150 mM KCl). It is, therefore, possible that the association of Nop9 with preribosomes is salt labile.

The 90S preribosome contains a large number of protein factors, most of which are not retained in the later pre-40S particles. The finding that Nop9 associates with both 90S and pre-40S particles indicates that additional, previously unidentified, factors are retained during this transition. In addition to known 90S and pre-40S ribosome synthesis factors, mass spectrometry on the Nop9-TAP precipitates identified several 60S subunit synthesis factors. It seems very likely that the late 90S particles will have assembled with at least some of the 60S synthesis factors. It is probable that some 60S factors bind prior to cleavage at A_2—the 3′ region of the 35S pre-rRNA cannot be naked RNA.

Depletion of Nop9 resulted in a 35S pre-rRNA processing defect similar to that of many other 90S components, with loss of the early cleavages at A_0, A_1, and A_2. This resulted in the failure to synthesize 18S rRNA, which is presumably the cause of lethality, while synthesis of the 25S and 5.8S rRNA species continued. As previously observed, alternative processing of the 35S at the A_3 site within ITS1 occurred when A_0, A_1, and A_2 were inhibited, resulting in accumulation of the aberrant 23S RNA species.

The finding that Nop9 does associate with preribosomes and is required for their biogenesis suggests that it and other such factors may comprise a new class of ribosome synthesis factors that associate in a transient or weak manner and are resistant to identification by conventional coprecipitation techniques.

The 20S pre-rRNA is generated in the nucleolus but is rapidly exported to the cytoplasm, where its maturation to 18S rRNA is completed. Nop9-GFP was localized solely to the nucleolus, suggesting that Nop9 does not accompany the pre-40S particles to the cytoplasm. This would be consistent with a transient association with the pre-40S particles. To study the localization of preribosomal particles, on depletion of Nop9 FISH was performed using fluorescently labeled oligonucleotide probes that decorate the pre-rRNAs. A probe complementary to the 5′ region of ITS1 (between sites D and A_2) recognizes 90S and pre-40S ribosomal particles. In wild-type cells, this probe localized to both the nucleus and cytoplasm but showed enrichment in the nucleolus. On depletion of Nop9, the ITS1 signal was markedly increased within the nucleolus, coupled with

a decrease in nucleoplasmic and cytoplasmic levels. This indicates that the defective 90S and/or pre-40S particles were retained in the nucleolus. The population of pre-rRNAs that accumulate and is decorated by the ITS1 probe is likely to be heterogeneous, as both 35S and 23S rRNA species were shown to accumulate at this time point by Northern analysis. It may be that release of preribosomal particles from the nucleolus to the nucleoplasm requires a signal, which reports that the correct stage of maturation has been achieved. Alternatively, preribosomes that have been identified as defective by surveillance systems could be actively retained in the nucleolus. The presence of aberrant RNP particles, containing 23S RNA and/or 35S pre-rRNA, might be among the signals recognized. Regardless of the specific mechanism, we hypothesize that preribosomal particles generated on depletion of Nop9 are aberrant and are consequently retained in the nucleolus for degradation.

Sequence analysis of Nop9 identified a pumilio-like domain and suggested that it might be capable of binding RNA. Numerous factors containing pumilio-like homology domains are implicated in the regulation of translation and mRNA stability and have been identified from yeast to mammals (Zamore et al. 1997; Zhang et al. 1997; Crittenden et al. 2002). From X-ray crystal structures, the pumilio homology domain was found to contain eight PUM repeats that pack together to form a right-handed super helix (Wang et al. 2001). The concave surface of this helix makes contact with the RNA via the individual PUM repeats with the outer surface of the domain believed to mediate protein–protein interactions. In vitro synthesized ^{35}S-labeled Nop9 efficiently bound homopolymeric poly(A) and poly(U) as well as natural RNA sequences, including a D-A_2 fragment, which forms the 3′ region of the 20S pre-rRNA, and in vitro transcribed $tRNA^{Met}$. The D-A_2 fragment was selected for analysis since affinity purification studies showed that Nop9-TAP precipitated 20S pre-rRNA but not mature 18S rRNA. However, Nop9 displayed no clear binding preference for the pre-rRNA over the highly structured tRNA. The authentic substrate is likely to be an RNA–protein complex, and this may be important for high affinity binding. Alternatively, as the binding of Nop9 seemed very good for all RNAs, it may be that in vivo specificity reflects the restriction of an otherwise promiscuous RNA binding activity.

MATERIALS AND METHODS

Strains and microbiological techniques

Standard procedures were used for the propagation and maintenance of yeast. A full list of strains used in this study can be found in Table 2. YET10 and YET12 were constructed using a one-step PCR strategy. Transformants were selected for resistance to G418 and were screened by PCR and immunoblotting. For pulse chase analyses, strains were transformed with a p*ADE2* vector to confer adenine prototrophy. For depletion of *GAL1*-regulated Nop9, cells were pregrown on permissive media containing 2% galactose and harvested immediately prior to transfer (0 h samples) and at time intervals following transfer to nonpermissive media containing 2% glucose.

Sucrose gradient analysis

Sucrose gradient analysis was performed on a 10%–50% gradient as previously described (Tollervey et al. 1993). RNA and protein was extracted from each fraction. RNA was resolved on a 1.2% agarose gel, where the RNA was denatured in glyoxyl, or on a 6% polyacrylamide/8.3 M urea gels. For analysis of Nop9-TAP, aliquots of each fraction were TCA-precipitated and resolved using standard SDS-PAGE techniques. The sedimentation profile of Nop9-TAP was detected by immunoblotting with a peroxidase-conjugated rabbit IgG (Sigma).

Affinity purification of Nop9-TAP

Affinity purification of Nop9-TAP was performed as previously described (Rigaut et al. 1999) with the following modifications. Batch binding of Nop9-TAP to IgG was carried out in 100 mM NaCl, 50 mM Tris (pH 7.4), 0.1% NP-40, protease inhibitor cocktail, and RNasin for 2 h at 4°C. TEV cleavage was performed in the same buffer minus the protease inhibitors and with the addition of 1 mM DTT and 100 U of AcTEV protease (Invitrogen) for 2 h at 18°C. Associated pre-rRNAs were recovered from the TEV eluate by GTC/PCA extraction and ethanol precipitation. RNA was analyzed by agarose/acrylamide gel electrophoresis and subsequent Northern hybridization.

A two-step TAP purification was performed to identify the proteins associated with Nop9-TAP, based on the technique previously described (Rigaut et al. 1999) with the following modifications. Sixteen grams of frozen yeast pellet, obtained from exponentially growing cells (OD_{600} 0.6), were ground in liquid nitrogen and thawed in extraction buffer (50 mM HEPES at pH 7.4, 50 mM KCl, 5 mM $MgCl_2$, 10% glycerol). Clarified extract was incubated with IgG sepharose for 1.5 h at 4°C. Washes and TEV cleavage were performed in buffer containing 50 mM HEPES, 100 mM KCl, 5 mM $MgCl_2$, 0.1% NP40, and 1 mM DTT. Calmodulin binding and release were performed as previously described (Rigaut et al. 1999).

TABLE 2. Strains used and constructed in this study

Strain	Genotype	Reference
BMA38	MATa *his3Δ200,leu2–3,112, ura3–1, trp1Δ, ade2–1*	(Baudin et al. 1993)
BY4741	MATa his3*Δ1, leu2Δ0, met15Δ0, ura3Δ0*	(Brachmann et al. 1998)
YET6	As BMA38 but *pAde*	This study
YET10	As BMA38, but *KAN::GAL1::3HA-Yjl010c*	This study
YET11	As BY4741, but *yjl010c-TAP::HIS*	(Ghaemmaghami et al. 2003)
YET 12	As BMA38 but *yjl010c-eGFP::HIS*	This study
YET13	As YET10, but *pAde*	This study

SDS-PAGE analysis and in-gel digestion

The entire lane of the silver-stained gel was divided into five fractions that were chopped into small pieces and placed in a 96-well plate for trypsin digestion as described elsewhere (Shevchenko et al. 1996). In brief, proteins were reduced in 20 mM DTT for 30 min at 37°C, alkylated in 50 mM iodoacetamide for 30 min at room temperature in the dark, and digested overnight at 37°C with 12.5 ng/μL trypsin (Proteomics Grade, Sigma). The digestion media were then acidified to 0.1% of TFA and spun onto StageTips as described elsewhere (Rappsilber et al. 2003). Peptides were eluted in 20 μL of 80% acetonitrile and 0.5% acetic acid and were concentrated to 2 μL (Concentrator 5301, Eppendorf AG). They were then diluted to 5 μL by 0.1% TFA for LC-MS/MS analysis.

Mass spectrometry analysis

An LTQ-Orbitrap mass spectrometer (ThermoElectron) was coupled online to an Agilent 1100 binary nanopump and an HTC PAL autosampler (CTC). To prepare an analytical column with a self-assembled particle frit (Ishihama et al. 2002), C_{18} material (ReproSil-Pur C18-AQ 3 μm; Dr. Maisch, GmbH) was packed into a spray emitter (75-μm ID, 8-μm opening, 70-mm length; New Objectives) using an air-pressure pump (Proxeon Biosystems). Mobile phase A consisted of water, 5% acetonitrile, and 0.5% acetic acid; mobile phase B, consisited of acetonitrile and 0.5% acetic acid. The gradient went from 0% to 20% buffer B in 75 min and then to 80% B in 13 min at 300 nL/min flow. The six most intense peaks of the MS scan were selected in the ion trap for MS^2, (normal scan, wideband activation, filling 5e5 ions for MS scan, 10^4 ions for MS^2, maximum fill time 100 msec, dynamic exclusion for 180 sec). Raw files were processed using DTAsupercharge 0.62 (a kind gift from Matthias Mann, Max Planck Institute of Biochemistry, Martinsried, Germany). The generated peak lists were searched against the SGD database (version 11.05.2007) using Mascot 2.0 with the parameters: monoisotopic masses, 8 ppm peptide tolerance and 0.6 Da MS/MS tolerance, ESI TRAP parameters, fully tryptic specificity, cysteine carbamidomethylated as fixed modification, oxidation on methionine as variable modification, with two missed cleavage sites allowed. The results were parsed through MSQuant (http://msquant.sourceforge.net/), and a cutoff 5-ppm peptide tolerance was applied to the recalibrated list. Peptides with scores 25 and higher were reported and in individual cases manually validated.

Pulse chase analysis

Metabolic labeling of pre-rRNA was performed as previously described (Tollervey et al. 1993) with the following modifications. The strains *BMA38* and *GAL::3HA-nop9* were transformed with a plasmid containing *ADE2* gene (strains YET6 and YET13). Strains were pregrown in synthetic galactose medium lacking adenine, and transferred to synthetic glucose medium lacking adenine for 8 h. Cells with an OD_{600} 0.4 were labeled with [8-^{3}H] adenine for 2 min followed by a chase of excess cold adenine. One-milliliter samples were spun down, and cell pellets were frozen in liquid nitrogen. RNA was extracted and ethanol precipitated.

RNA extraction and Northern hybridization

RNA was extracted as previously described (Tollervey and Mattaj 1987). For high-molecular-weight RNA analysis 4 μg of total of RNA was glyoxyl denatured and resolved on a 1.2% agarose gel, as previously described (Sambrook and Russell 2001). Low-molecular-weight RNAs were resolved on standard 6% Acrylamide/8.3 M urea gels. The positions of oligonucleotides used for Northern hybridizations are shown in Figure 1A, and the sequences are listed in Table 3.

Immunofluoresence and fluorescence in situ hybridization

For immunofluorescence and FISH, cells were fixed in 3.7% paraformaldehyde at room temperature, spheroplasted using zymolase, and dehydrated in 70% ethanol overnight at −20°C. Fluorescence in situ hybridization was performed as previously described (Long et al. 1995). Oligonucleotide probes containing aminomodified deoxythymidine residues (amino-C6-dT) were labeled with a ULS Cy-3 kit (GE Amersham). The sequences of the probes used are ITS1-TT*GCACAGAAATCTCT*CACCGT TTGGAAT*AGCAAGAAAGAAACT*TACAAGCT*T and ITS2-AT* AGGCCAGCAATTTCAAGTT*AACTCCAAAGAGTATCACT*C, where T* represents amino-C6-dT. Nop1p was detected with a mouse anti-Nop1 antibody (kindly provided by J. Aris, University of Florida, Gainesville, FL), and a secondary goat anti-mouse antibody conjugated to Alexafluor 488 or 555 (Molecular Probes). To stain nuclear DNA, DAPI was included in the mounting medium (Vectashield, Vector laboratories).

Nop9-GFP localization studies were performed on a Leica DMR fluorescence microscope, and images were captured using a Coolsnap CCD camera. Images for FISH experiments were captured using a coolsnap CCD camera fitted to the DeltaVision RT Restoration Imaging System. Images captured using the DeltaVision system were subjected to real-time, two-dimensional deconvolution algorithms. Single optical sections were selected following deconvolution and assembled using ImageJ software.

RNA binding assays

Binding of [^{35}S]-Nop9 to homopolymeric nucleotides, and biotinylated, in vitro transcribed RNA was performed as previously described (Rexach and Blobel 1995; Oeffinger et al. 2004). Equivalent amounts of protein recovered from bound, unbound,

TABLE 3. Oligonucleotides used as hybridization probes

Oligo	Sequence (5′-3′)
003	TGCTTACCTCTGGGCC
004	CGGTTTTAATTGTCCTA
006	AGATTAGCCGCAGTTGG
007	CTCCGCTTATTGATATGC
008	CATGGCTTAATCTTTGAGAC
017	GCGTTGTTCATCGATGC
020	TGAGAAGGAAATGACGCT
033	CGCTGCTCACCAATGG
041	CTACTCGGTCAGGCTC
200	TTATGGGACTTGTT
202	TCACTCAGACATCCTAGG
225	CTCCCTAAAGCATCACAA
228	CATCCAGCTCAAGATCG
231	ATGTCTGCAGTATGGTTTTAC
250	ATCCCGGCCGCCTCCATCAC

and total fractions were separated by SDS-PAGE on a 4%–12% Bis-tris gel. Following migration, the gel was dried, and protein was visualized by autoradiography.

ACKNOWLEDGMENTS

We thank Flavia Alves for expert assistance with mass spectrometry. This work was supported by the Wellcome Trust. J.R. was the recipient of grant from the European Union.

Received July 20, 2007; accepted September 6, 2007.

REFERENCES

Allmang, C., Mitchell, P., Petfalski, E., and Tollervey, D. 2000. Degradation of ribosomal RNA precursors by the exosome. *Nucleic Acids Res.* **28:** 1684–1691. doi: 10.1093/nar/28.8.1684.

Baßler, J., Grandi, P., Gadal, O., Leßmann, T., Petfalski, E., Tollervey, D., Lechner, J., and Hurt, E. 2001. Identification of a 60S pre-ribosomal particle that is closely linked to nuclear export. *Mol. Cell* **8:** 517–529.

Baudin, A., Ozier-Kalogeropoulos, O., Denouel, A., Lacroute, F., and Cullin, C. 1993. A simple and efficient method for direct gene deletion in *Saccharomyces cerevisiae*. *Nucleic Acids Res.* **21:** 3329–3330. doi: 10.1093/nar/21.14.3329.

Brachmann, C.B., Davies, A., Cost, G.J., Caputo, E., Li, J., Hieter, P., and Boeke, J.D. 1998. Designer deletion strains derived from *Saccharomyces cerevisiae* S288C: A useful set of strains and plasmids for PCR-mediated gene disruption and other applications. *Yeast* **14:** 115–132.

Crittenden, S.L., Bernstein, D.S., Bachorik, J.L., Thompson, B.E., Gallegos, M., Petcherski, A.G., Moulder, G., Barstead, R., Wickens, M., and Kimble, J. 2002. A conserved RNA-binding protein controls germline stem cells in *Caenorhabditis elegans*. *Nature* **417:** 660–663.

Dragon, F., Gallagher, J.E., Compagnone-Post, P.A., Mitchell, B.M., Porwancher, K.A., Wehner, K.A., Wormsley, S., Settlage, R.E., Shabanowitz, J., Osheim, Y., et al. 2002. A large nucleolar U3 ribonucleoprotein required for 18S ribosomal RNA biogenesis. *Nature* **417:** 967–970.

Fatica, A., Cronshaw, A.D., Dlakic, M., and Tollervey, D. 2002. Ssf1p prevents premature processing of an early pre-60S ribosomal particle. *Mol. Cell* **9:** 341–351.

Ghaemmaghami, S., Huh, W.K., Bower, K., Howson, R.W., Belle, A., Dephoure, N., O'Shea, E.K., and Weissman, J.S. 2003. Global analysis of protein expression in yeast. *Nature* **425:** 737–741.

Grandi, P., Rybin, V., Bassler, J., Petfalski, E., Strauss, D., Marzioch, M., Schafer, T., Kuster, B., Tschochner, H., Tollervey, D., et al. 2002. 90S pre-ribosomes include the 35S pre-rRNA, the U3 snoRNP, and 40S subunit processing factors but predominantly lack 60S synthesis factors. *Mol. Cell* **10:** 105–115.

Harnpicharnchai, P., Jakovljevic, J., Horsey, E., Miles, T., Roman, J., Rout, M., Meagher, D., Imai, B., Guo, Y., Brame, C.J., et al. 2001. Composition and functional characterization of yeast 66s ribosome assembly intermediates. *Mol. Cell* **8:** 505–515.

Hazbun, T.R., Malmstrom, L., Anderson, S., Graczyk, B.J., Fox, B., Riffle, M., Sundin, B.A., Aranda, J.D., McDonald, W.H., Chiu, C.H., et al. 2003. Assigning function to yeast proteins by integration of technologies. *Mol. Cell* **12:** 1353–1365.

Ishihama, Y., Rappsilber, J., Andersen, J.S., and Mann, M. 2002. Microcolumns with self-assembled particle frits for proteomics. *J. Chromatogr.* **979:** 233–239.

Krogan, N.J., Cagney, G., Yu, H., Zhong, G., Guo, X., Ignatchenko, A., Li, J., Pu, S., Datta, N., Tikuisis, A.P., et al. 2006. Global landscape of protein complexes in the yeast *Saccharomyces cerevisiae*. *Nature* **440:** 637–643.

Long, R.M., Elliott, D.J., Stutz, F., Rosbash, M., and Singer, R.H. 1995. Spatial consequences of defective processing of specific yeast mRNAs revealed by fluorescent in situ hybridization. *RNA* **1:** 1071–1078.

Oeffinger, M., Dlakic, M., and Tollervey, D. 2004. A pre-ribosome-associated HEAT-repeat protein is required for export of both ribosomal subunits. *Genes & Dev.* **18:** 196–209.

Perez-Fernandez, J., Roman, A., De Las Rivas, J., Bustelo, X.R., and Dosil, M. 2007. The 90s pre-ribosome is a multimodular structure that is assembled through a hierarchical mechanism. *Mol. Cell. Biol.* **27:** 5414–5429.

Rappsilber, J., Ishihama, Y., and Mann, M. 2003. Stop and go extraction tips for matrix-assisted laser desorption/ionization, nanoelectrospray, and LC/MS sample pretreatment in proteomics. *Anal. Chem.* **75:** 663–670.

Rexach, M. and Blobel, G. 1995. Protein import into nuclei: Association and dissociation reactions involving transport substrate, transport factors, and nucleoporins. *Cell* **83:** 683–692.

Rigaut, G., Shevchenko, A., Rutz, B., Wilm, M., Mann, M., and Seraphin, B. 1999. A generic protein purification method for protein complex characterization and proteome exploration. *Nat. Biotechnol.* **17:** 1030–1032.

Sambrook, J. and Russell, D.W. 2001. *Molecular cloning*. Cold Spring Harbor Laboratory Press, Cold Spring Harbor, NY.

Saveanu, C., Bienvenu, D., Namane, A., Gleizes, P.-E., Gas, N., Jacquier, A., and Fromont-Racine, M. 2001. Nog2p, a putative GTPase associated with pre-60S subunits and required for late 60S maturation steps. *EMBO J.* **20:** 6475–6484.

Saveanu, C., Namane, A., Gleizes, P.-E., Lebreton, A., Rousselle, J.-C., Noaillac-Depeyre, J., Gas, N., Jacquier, A., and Fromont-Racine, M. 2003. Sequential protein association with nascent 60S ribosomal particles. *Mol. Cell. Biol.* **23:** 4449–4460.

Schafer, T., Strauss, D., Petfalski, E., Tollervey, D., and Hurt, E. 2003. The path from nucleolar 90S to cytoplasmic 40S pre-ribosomes. *EMBO J.* **22:** 1370–1380.

Shevchenko, A., Wilm, M., Vorm, O., and Mann, M. 1996. Mass spectrometric sequencing of proteins from silver-stained polyacrylamide gels. *Anal. Chem.* **68:** 850–858.

Tollervey, D. and Mattaj, I.W. 1987. Fungal small nuclear ribonucleoproteins share properties with plant and vertebrate U-snRNPs. *EMBO J.* **6:** 469–476.

Tollervey, D., Lehtonen, H., Jansen, R., Kern, H., and Hurt, E.C. 1993. Temperature-sensitive mutations demonstrate roles for yeast fibrillarin in pre-rRNA processing, pre-rRNA methylation, and ribosome assembly. *Cell* **72:** 443–457.

Udem, S.A. and Warner, J.R. 1973. The cytoplasmic maturation of a ribosomal precursor ribonucleic acid in yeast. *J. Biol. Chem.* **248:** 1412–1416.

Wang, X., Zamore, P.D., and Hall, T.M. 2001. Crystal structure of a pumilio homology domain. *Mol. Cell* **7:** 855–865.

Winzeler, E.A., Shoemaker, D.D., Astromoff, A., Liang, H., Anderson, K., Andre, B., Bangham, R., Benito, R., Boeke, J.D., Bussey, H., et al. 1999. Functional characterization of the *S. cerevisiae* genome by gene deletion and parallel analysis. *Science* **285:** 901–906.

Wu, P., Brockenbrough, J.S., Metcalfe, A.C., Chen, S., and Aris, J.P. 1998. Nop5p is a small nucleolar ribonucleoprotein component required for pre-18 S rRNA processing in yeast. *J. Biol. Chem.* **273:** 16453–16463.

Zamore, P.D., Williamson, J.R., and Lehmann, R. 1997. The pumilio protein binds RNA through a conserved domain that defines a new class of RNA-binding proteins. *RNA* **3:** 1421–1433.

Zhang, B., Gallegos, M., Puoti, A., Durkin, E., Fields, S., Kimble, J., and Wickens, M.P. 1997. A conserved RNA-binding protein that regulates sexual fates in the *C. elegans* hermaphrodite germ line. *Nature* **390:** 477–484.